EPJ Web of Conferences **125**, 04010 (2016) DOI: 10.1051/epjconf/201612504010
QUARKS-2016

Hydro and Jets in Relativistic Heavy-Ion Collisions

L.V. Bravina[1,3,4,a], B.H. Brusheim Johansson[1], J. Crkovská[5,6], G.Kh. Eyyubova[2,7], V.L. Korotkikh[2], I.P. Lokhtin[2], L.V. Malinina[2,7], E.N. Nazarova[2], S.V. Petrushanko[2], A.M. Snigirev[2], and E.E. Zabrodin[1,2,3,4]

[1] *Department of Physics, University of Oslo, PB 1048 Blindern, N-0316 Oslo, Norway*
[2] *Skobeltsyn Institute of Nuclear Physics, Moscow State University, RU-119991 Moscow, Russia*
[3] *Frankfurt Institute for Advanced Studies, Ruth-Moufang-Str. 1, D-60438 Frankfurt a.M., Germany*
[4] *National Research Nuclear University "MEPhI" (Moscow Engineering Physics Institute), RU-115409 Moscow, Russia*
[5] *Czech Technical University in Prague, FNSPE, CR-11519 Prague, Czech Republic*
[6] *Institut de Physique Nucléaire, CNRS-IN2P3, Univ. Paris-Sud, Université Paris-Saclay, F-91406 Orsay Cedex, France*
[7] *Joint Institute for Nuclear Researches, Dubna, Russia*

Abstract. We apply HYDJET++ model, which contains the treatment of both soft and hard processes, to study the heavy-ion collisions at LHC energies. The interplay of parametrised hydrodynamics and jets describes many features of the development of particle anisotropic flow including the break-up of mass hierarchy of elliptic and triangular flow, the falloff of the flow at certain transverse momentum and violation of the number-of-constituent-quark (NCQ) scaling at LHC energies compared to the lower ones. Other signals, such as long-range dihadron correlations (ridge) and event-by-event (EbyE) fluctuations of the flow are also discussed. Model calculations demonstrate a good agreement with the available experimental data.

1 Introduction

The main difficulties emerging in analysis of data on relativistic heavy-ion collisions (HIC's) are (i) absence of the unified theory for the description of these collisions, (ii) that perturbative quantum chromodynamics (QCD) does not apply for "soft" interactions with small transverse momentum transfer, which play an essential role in physics of HIC's, and (iii) that the final state of HIC's is very complicated to extract easily the signatures of the new state of matter, the quark-gluon plasma (QGP). Therefore, models are indispensable for evaluating the current experiments and for planing the new ones. These models can be subdivided into macroscopic, i.e. thermal [1–3] and hydrodynamic models [4–6], and microscopic Monte Carlo models [7–10], incorporating partonic and hadronic degrees of freedom in a consistent fashion. Note that for better description of data, hydrodynamic models nowadays are employing the microscopic transport models as afterburner.

[a] e-mail: larissa.bravina@fys.uio.no

In contrast to microscopic transport models, macroscopic models usually deal with soft processes with particle transverse momentum up to $p_T \approx 1.5 - 2$ GeV/c only, and do not include jets. HYDJET++ model [11] was, probably, the first attempt to combine a hydro-like state and hard processes within a single event generator. This idea appears to be very promising. After the discussion of basic principles of the model in Sec. 2, the most interesting results obtained by the HYDJET++ are listed in Sec. 3. Finally, conclusions are drawn in Sec. 4.

2 HYDrodynamics with JETs (HYDJET++)

In HYDJET++ the soft state is represented by a hydro-like system [12, 13]. It is coupled to a hard multiparton state, where the hard partons are suffering the collisional and gluon radiation losses [14] when propagating the dense and hot medium. For the sake of simplicity, both states are treated independently. In the soft sector sector HYDJET++ employs the popular Bjorken or Hubble expansion scenarios for the overlapping zone of heavy-ion collisions. At certain temperature $T = T^{ch}$ and chemical potentials μ_i, where $i = B, S, Q$ represents baryon charge, strangeness and electric charge, respectively, the thermalised fireball breaks into individual hadrons in a sudden chemical freeze-out process. The particle number density $\rho_i^{eq}(T, \mu_i)$ is given by the well-known series expansion [4]

$$\rho_i^{eq}(T, \mu_i) = \frac{g_i}{2\pi^2} m_i^2 T \sum_{k=1}^{\infty} \frac{(\mp)^{k+1}}{k} \exp\left(\frac{k\mu_i}{T}\right) K_2\left(\frac{km_i}{T}\right) , \tag{1}$$

where g_i is the spin degeneracy factor, m_i is the particle mass, and K_2 is the modified Bessel function of a second kind. To calculate the particle yields one has to know the fireball volume. It is proportional to the mean number of wounded nucleons at a given impact parameter b , see [11–13] for details. After the chemical freeze-out, the system of hadrons continues to expand until the thermal contact between the particles is lost. This is the stage of thermal freeze-out. The only final-state interactions taken into account in the model are two- and three-body decays of resonances. HYDJET++ benefits from the extensive table of particles which contains more than 360 meson and baryon states including the charmed ones. The mass distribution of the resonances is given by a non-relativistic Breit-Wigner formula

$$P(m)dm \propto \frac{1}{(m - m_0)^2 + \Delta m^2/4} dm , \tag{2}$$

where m_0 and Δm are the resonance nominal mass and width, respectively.

The hard multiparton stage emerges in the model as a superposition of individual hard nucleon-nucleon (NN) collisions. For each collision, the PYQUEN routine [14] generates the initial parton spectra (by means of the tune Pro-Q20 of PYTHIA [15]) and the production vertexes. The parton rescattering stage is accompanied by collisional energy loss and radiation of gluons. In high-momentum transfer limit, the collisional loss reads

$$\frac{dE}{dl}^{col} = \frac{1}{4T\lambda\sigma} \int_{\mu_D^2}^{t_{\max}} dt \frac{d\sigma}{dt} t , \tag{3}$$

with the dominant contribution to the differential scattering cross section

$$\frac{d\sigma}{dt} \cong C \frac{2\pi\alpha_s^2(t)}{t^2} \frac{E^2}{E^2 - m_p^2} . \tag{4}$$

Here $\lambda = 1/(\sigma\rho)$ is the mean free path of a parton in a medium with density ρ and integral cross section of parton-medium interaction σ. In the last equation E and m_p are energy and mass of the parton, α_s is the QCD running coupling constant, and $C = 4/9, 1, 9/4$ for qq, gq and gg interaction, respectively. Then, the energy spectrum of coherent medium-induced gluon radiation and the corresponding dominant part of radiative energy loss of massless parton in the framework of BDMS formalism [16, 17] become

$$\frac{dE^{rad}}{dl} = \frac{2\alpha_s(\mu_D^2)C_R}{\pi L}\int\limits_{\omega_{\min}}^{E} d\omega\left[1-y+\frac{y^2}{2}\right]\ln\left|\cos\left(\omega_1\tau_1\right)\right|, \tag{5}$$

$$\omega_1 = \sqrt{i\left(1-y+\frac{C_R}{3}y^2\right)\bar{\kappa}\ln\frac{16}{\bar{\kappa}}} \quad \text{with} \quad \bar{\kappa} = \frac{\mu_D^2\lambda_g}{\omega(1-y)}, \tag{6}$$

containing $\tau_1 = L/(2\lambda_g)$, λ_g is the gluon mean free path, and $y = \omega/E$ is the parton energy fraction carried away by the gluon. Partons produced in initial hard scatterings with the transverse momentum transfer lower than a certain limit p_{T}^{min} are excluded from the hard component. Their hadronization products are added to the thermalised component of particle spectrum.

Let us discuss generation of the anisotropic flow in non-central heavy ion collisions in the model. Recall, that the flow harmonics are the Fourier coefficients of series expansion of the invariant cross section in azimuthal plane [18]

$$E\frac{d^3N}{d^3p} = \frac{1}{\pi}\frac{d^2N}{dp_T^2dy}\left\{1+2\sum_{n=1}^{\infty}v_n\cos\left[n(\phi-\Psi_n)\right]\right\}, \tag{7}$$

$$v_n = \langle\cos\left[(n(\phi-\Psi_n)\right]\rangle. \tag{8}$$

Here y is the particle rapidity, ϕ is the azimuthal angle between the particle transverse momentum p_T and the participant plane, and Ψ_n is the azimuth of the participant plane of n-th order. The flow harmonic coefficients are called directed, v_1, elliptic, v_2, triangular, v_3, quadrangular, v_4, pentagonal, v_5, hexagonal, v_6, flow and so forth. The transverse radius of the fireball for non-central heavy ion collision depends on impact parameter b, azimuthal angle ϕ and spatial eccentricity $\epsilon(b) = (R_y^2 - R_x^2)/(R_y^2 + R_x^2)$ as [13]

$$R_{ell}(b,\phi) = R_{fr.-out}(b)\sqrt{\frac{1-\epsilon^2(b)}{1+\epsilon(b)\cos 2\phi}}. \tag{9}$$

The parameter $R_{fr.-out}(b)$ is linked to the freeze-out radius of the fireball in a central collision, R_0, as $R_{fr.-out}(b) = R_0\sqrt{1-\epsilon(b)}$. The momentum anisotropy arises from the pressure gradients, which are stronger in the direction of short axis of the ellipsoid. Another free parameter, $\delta(b)$, connects the flow azimuthal angle ϕ_{fl} with the azimuthal angle ϕ. Namely,

$$\delta(b) = \frac{1-C^2}{1+C^2}, \quad C = \frac{\tan\phi_{fl}}{\tan\phi}. \tag{10}$$

Triangular flow needs further modification of the transverse radius [20], which is controlled by new free parameter $\epsilon_3(b)$

$$R_{triang}(b,\phi) = R_{ell}(b,\phi)\{1+\epsilon_3(b)\cos\left[3(\phi-\Psi_3)\right]\}. \tag{11}$$

According to experimental data, elliptic and triangular flow are not correlated in the model. Further details of HYDJET++ can be found in [11–13].

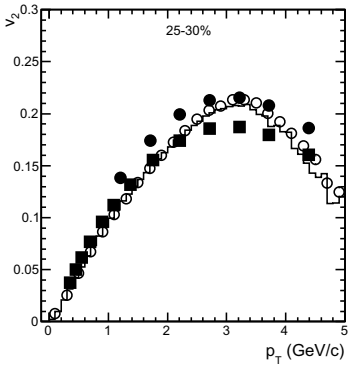

Figure 1. The $v_2(p_T)$ distributions in the HYDJET++ model for 25-30% centrality collisions (histogram) compared to event-plane flow restoration method (open circles) and CMS data (full symbols). See text for details.

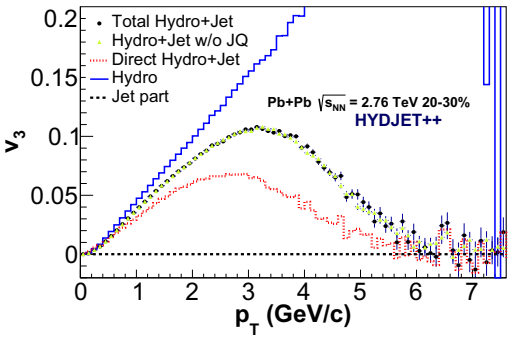

Figure 2. The $v_3(p_T)$ distributions for charged hadrons from (i) all processes (solid circles), (ii) soft+hard processes w/o jet quenching (open triangles), (iii) directly frozen hadrons (dash-dotted line), (iv) soft processes (solid histogram), (v) jets (dashed line) in Pb+Pb at 2.76 TeV with centrality 20-30%.

3 Interplay of soft processes and jets

For our further analysis Pb+Pb collisions at $\sqrt{s} = 2.76$ TeV are chosen. Figure 1 displays elliptic flow of charged hadrons produced in collisions with centrality 25-30%. Experimental data by the CMS Collaboration [19] obtained by the 2-cumulant and Lee-Yang zeroes (LYZ) methods are plotted also. To estimate possible distortion of the flow spectra caused by the reconstruction procedure, the generated particle spectra were used as an input for the flow determination. The event-plane (EP) method was employed. The restored spectrum is very close to the original one. Model calculations agree well with the data. The good agreement with the experiment is obtained for the triangular flow and higher flow harmonics as well, see [20].

Note that falloff of the differential flow $v_2(p_T)$ at $p_T \geq 3$ GeV/c is a common feature of all flow harmonics. Since we apply ideal parameterised hydrodynamics which has no such peculiarity, the most plausible explanation of the drop of $v_n(p_T)$ is the jet influence. One can see this in Fig. 2, which shows the partial contributions of different subprocesses to the triangular flow $v_3(p_T)$ in collisions with centrality 20-30%. In addition to the total v_3, this figure presents also the flow in case of absence of jet-medium interaction, flow of particles produced merely in soft processes, flow of particles without the resonance feed-down, and flow of hadrons decoupled from jets. The latter is essentially zero, whereas its hydrodynamic counterpart increases with rising p_T. After certain transverse momentum, however, the total spectrum of hadrons is dominated by particles produced in hard processes which can carry very weak flow because of the jet quenching [21]. Since these particles prevail in the hadron spectrum, the total flow drops.

The same mechanism explains also violation of the meson-baryon hierarchy in p_T-differential $v_n(p_T)$, seen in Fig. 3. This figure depicts the triangular flow of most abundant charged hadrons, i.e. pions, $\pi^{\pm}$, kaons, $K^{\pm}$, and (anti)protons, $p+\bar{p}$. At transverse momenta below 2 GeV/c, triangular flow of mesons is stronger than the flow of $p + \bar{p}$. Moreover, in ideal hydrodynamics $v_3(p_T)$ of different hadron species do not cross each other. But then jets come into play. For a given hadron species the crossing point of hard and soft parts of its p_T-spectrum depends on the hadron mass. The heavier the hadron, the larger the transverse momentum at which the jet-produced particles become more

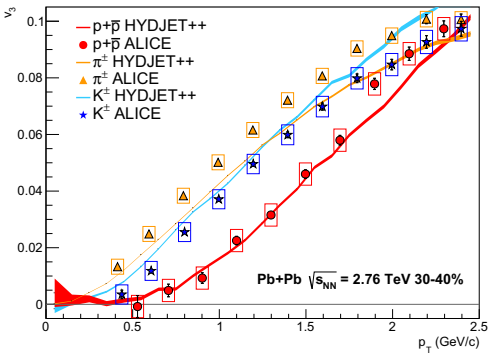

Figure 3. p_T-differential triangular flow of charged pions, kaons, and protons plus antiprotons in Pb+Pb collisions at 2.76 TeV with centrality 20-30%. solid curves indicate HYDJET++ calculations, symbols show ALICE data from [22].

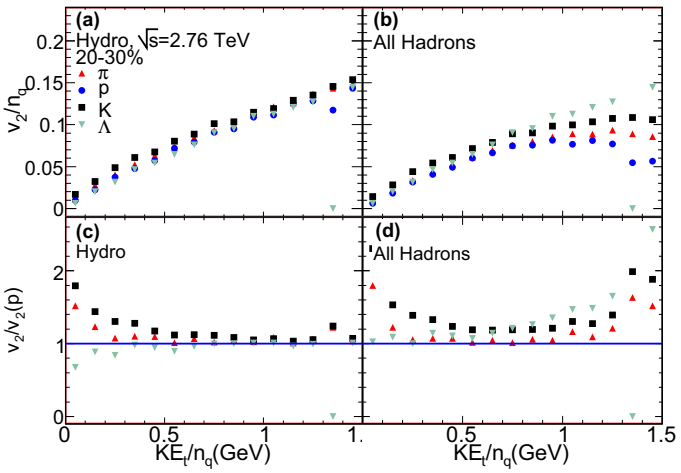

Figure 4. Upper row: The KE_T/n_q dependence of elliptic flow for (a) hadrons produced in soft processes only, and (b) all hadrons calculated in HYDJET++ model for Pb+Pb collisions at 2.76 TeV with centrality 20-30%. Bottom row: The distributions from the upper row are normalised to the elliptic flow of $p + \bar{p}$.

abundant. Therefore, the p_T-differential flow of mesons experiences the saturation and subsequent drop at smaller p_T compared to heavier baryons. This effect is called violation of the mass ordering of the flow.

Also, increasing number of hard processes with the rise of collision energy of heavy ions explains the worsening of the number-of-constituent-quark scaling of elliptic flow at LHC. The effect was first observed in Au+Au collisions at RHIC [23, 24]. If the elliptic flow v_2 and the transverse kinetic energy $KE_T = m_T - m_0$ are divided by a number of constituent quarks n_q, 3 for baryons and 2 for mesons, then the distributions $v_2/n_q(KE_T/n_q)$ for all hadrons coincide with good accuracy up to $KE_T/n_q \approx 1$ GeV. This circumstance was taken as a strong evidence of the predominant production of

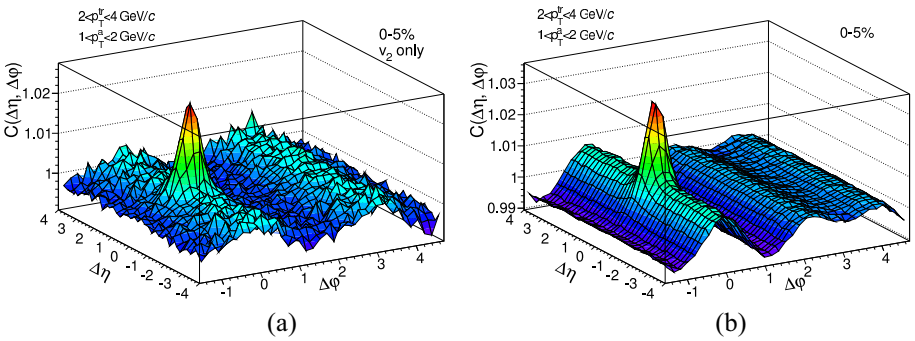

Figure 5. 2D correlation function in HYDJET++ in Pb+Pb collisions at $\sqrt{s_{\rm NN}}$ = 2.76 TeV for $2 < p_{\rm T}^{\rm tr} < 4$ GeV/c and $1 < p_{\rm T}^{\rm a} < 2$ GeV/c for centrality 0-5% with (a) only elliptic flow and (b) with both elliptic and triangular flow.

elliptic flow from the quark coalescence at the partonic stage, most presumably, quark-gluon plasma (QGP). The violation of NCQ scaling was predicted by HYDJET++ [25, 26] before its experimental observation by the ALICE Collaboration [27].

The reduced functions $v_2(KE_T/n_q)/n_q$ of $\pi^{\pm}, K^{\pm}, p$ and Λ calculated in HYDJET++ for 20-30% central Pb+Pb collisions at 2.76 TeV are shown in Fig. 4. Left upper panel displays the results for the soft sector. As one can see, all distributions are indeed on the top of each other up to 1.5 GeV. To see the degree of the scaling fulfillment explicitly all particle flows in the bottom row are normalized to the flow of protons, $v_2^h/n_q : v_2^p/n_q$. Hadrons from jets make the scaling performance significantly worse, as seen im right panels of Fig. 4. The NCQ scaling at LHC holds only approximately within the range $0.4 \leq KE_T/n_q \leq 0.8$ GeV despite the fact that in pure hydrodynamic sector with final state interactions the scaling fulfillment is very good. The detailed study of consequences of the interplay between the soft processes and jets on the development of elliptic and triangular flow and higher order harmonics within the HYDJET++ can be found in [20, 25, 26, 28–31].

Finally, we would like to discuss the issue of correlations and fluctuations presented in the model. Among the sources of particle correlations in HYDJET++ are decays of resonances, jets, femtoscopic correlations, correlations imposed by energy-momentum conservation and so forth. However, as was shown in [32], the long-range correlations arise in the model merely because of the collective flow. The di-hadron correlation function $C(\Delta\eta, \Delta\varphi)$, where $\Delta\eta = \eta^{tr} - \eta^{a}$ and $\Delta\varphi = \varphi^{tr} - \varphi^{a}$ is presented in Fig. 5(a,b) for the calculations of Pb+Pb collisions with centrality 0-5%. - The indices “tr" and “a" indicate the so-called “trigger" and “associated" particle, respectively. - Two cases are considered: (a) without and (b) with the triangular flow in addition to the elliptic one. We see that the long-range azimuthal correlations appear both at near-side ($\Delta\varphi \approx 0$) and at away-side ($\Delta\varphi \approx \pi$) in both figures. But the experimentally observed [33, 34] double-hump structure at the away-side emerges in the model only in the presence of elliptic and triangular flow simultaneously.

The event-by-event (EbyE) distributions of anisotropic flow harmonics in Pb+Pb collisions at LHC were studied by ATLAS Collaboration in [35] by means of the *unfolding* procedure. This method suppresses strongly the non-flow effects caused, e.g. by decays of resonances, finite event multiplicity or jet fragmentation. To get rid of such effects, unfolding was implemented in our study of the EbyE flow fluctuations within the HYDJET++ in [36]. Results are shown in Fig. 6, where the model calculations of probability density distributions of elliptic and triangular EbyE flow are compared with the ATLAS data. Agreement is good. Initial $P(V_n)$ distributions are broader than the unfolded ones; unfolding

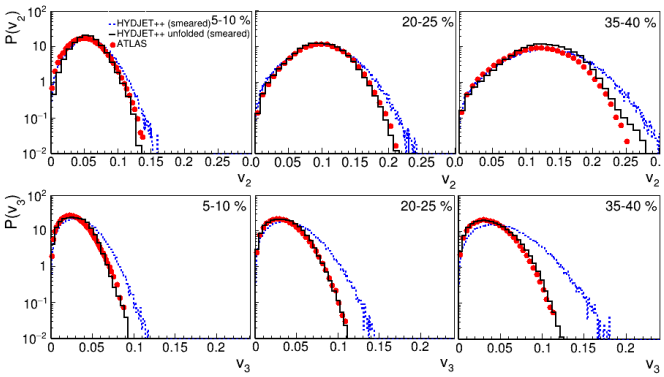

Figure 6. The probability density distributions of elliptic flow V_2 (upper row) and triangular flow V_3 (bottom row) in three centrality intervals: 5 – 10% (left), 20 – 25% (middle) and 35 – 40% (right). Dashed and solid histograms present the results for simulated HYDJET++ events before and after the unfolding procedure, respectively. The full circles are the ATLAS data from [35].

procedure makes it narrower. Obtained results strongly support the idea of dynamical origin of the EbyE flow fluctuations in the model.

4 Conclusions

We show the importance of hard processes for the correct treatment of anisotropic flow harmonics in heavy-ion collisions at ultrarelativistic energies within the ideal hydrodynamic model. Jets account for (i) falloff of the flow harmonics in the range of intermediate transverse momenta, (ii) changing of the mass ordering of the hadron elliptic and triangular flow, and (iii) the violation of the number-of-constituent-quark scaling at energies of LHC and higher.

The interplay between v_2 and v_3 is able to describe both qualitatively and quantitatively the di-hadron long-range correlations, i.e. ridge at near-side and double-hump structure at the away-side. The unfolding procedure was employed to study event-by-event flow fluctuations in the model and compare the obtained results with the experimental data. The comparison revealed dynamical origin of the flow fluctuations, originating primarily from the correlation between the momenta and coordinates of final particles and the velocities of hadronic fluid elements.

Acknowledgments

This work was supported in parts by the Grant INGO II LG15001 of the Ministry of Education, Youth and Sports of the Czech Republic and the Grant Agency of Czech Republic No.13-20841S, and the Grant of the President of Russian Federation for Scientific Schools Supporting No. 7989.2016.2. L.B. acknowledges financial support of the Alexander von Humboldt Foundation.

References

[1] E. Fermi, Prog. Theor.Phys. **5**, 570 (1950)

[2] G. Torrieri *et al.*, Comput. Phys. Commun. **167**, 229 (2005)
[3] A. Kisiel, T. Taluc, W. Broniowski, and W. Florkowski, Comput. Phys. Commun. **174**, 669 (2006)
[4] L. D. Landau, Izv. Akad. Nauk Ser. Fiz. **17**, 51 (1953);
S. Z. Belenkij and L. D. Landau, Nuovo Cim. Suppl. **3S10**, 15 (1956)
[5] H. Song, S. A. Bass, and U. Heinz, Phys. Rev. C **83**, 024912 (2011)
[6] B. Schenke, S. Jeon, and C. Gale, Phys. Rev. C **82**, 014903 (2010)
[7] A. Capella, U. Sukhatme, C.-I. Tan, and J. Tran Thanh Van, Phys. Rep. **236**, 225 (1994)
[8] S. A. Bass *et al.*, Prog. Part. Nucl. Phys. **41**, 255 (1998);
M. Bleicher *et al.*, J. Phys. G **25**, 1859 (1999)
[9] N. S. Amelin and L. V. Bravina, Sov. J. Nucl. Phys. **51**, 133 (1990);
E. E. Zabrodin, C. Fuchs, L. V. Bravina, and Amand Faessler, Phys. Lett. B **508**, 184 (2001);
J. Bleibel, L. V. Bravina, and E. E. Zabrodin, Phys. Rev. D **93**, 114012 (2016)
[10] Z.-W. Lin, *et al.*, Phys. Rev. C **72**, 064901 (2005)
[11] I. P. Lokhtin *et al.*, Comput. Phys. Commun. **180**, 779 (2009)
[12] N. S. Amelin *et al.*, Phys. Rev. C **74**, 064901 (2006)
[13] N. S. Amelin *et al.*, Phys. Rev. C **77**, 014903 (2008)
[14] I. P. Lokhtin and A. M. Snigirev, Eur. Phys. J. C **46**, 211 (2006)
[15] T. Sjostrand, S. Mrenna, and P. Skands, JHEP **0605**, 026 (2006)
[16] R. Baier, Yu. L. Dokshitzer, A. H. Mueller, and D. Schiff, Phys. Rev. C **60**, 064902 (1999)
[17] R. Baier, Yu. L. Dokshitzer, A. H. Mueller, and D. Schiff, Phys. Rev. C **64**, 057902 (2001)
[18] S. A. Voloshin and Y. Zhang, Z. Phys. C **70**, 665 (1996)
[19] S. Chatrchyan *et al.* (CMS Collaboration), Phys. Rev. C **87**, 014902 (2013)
[20] L. V. Bravina *et al.*, Eur. Phys. J. C **74**, 2807 (2014)
[21] X.-N. Wang and M. Gyulassy, Phys. Rev. Lett. **68**, 1480 (1992)
[22] J. Adam *et al.*, (ALICE Collaboration), arXiv:1606.06057 [nucl-ex]
[23] J. Adams *et al.* (STAR Collaboration), Phys. Rev. Lett. **92**, 052302 (2004)
[24] S. S. Adler *et al.* (PHENIX Collaboration), Phys. Rev. Lett. **91**, 182301 (2003)
[25] G. Eyyubova *et al.*, Phys. Rev. C **80**, 064907 (2009)
[26] E. Zabrodin *et al.*, J. Phys. G. **37**, 094060 (2010)
[27] F. Noferini *et al.* (ALICE Collaboration), Nucl. Phys. A **904-905**, 438c (2013)
[28] I. P. Lokhtin *et al.*, Eur. Phys. J. C **72**, 2045 (2012)
[29] L. Bravina, B. H. Brusheim Johansson, G. Eyyubova, and E. Zabrodin, Phys. Rev. C **87**, 034901 (2013)
[30] L. V. Bravina *et al.*, Phys. Rev. C **89**, 024909 (2014)
[31] J. Crkovská *et al.*, arxiv:1606.03250 [hep-ph]
[32] G. Eyyubova *et al.*, Phys. Rev. C **91**, 064907 (2015)
[33] K. Aamodt *et al.* (ALICE Collaboration), Phys. Rev. Lett. **107**, 032301 (2011)
[34] S. Chatrchyan *et al.* (CMS Collaboration), Eur. Phys. J. **C72**, 2012 (2012)
[35] G. Aad *et al.* (ATLAS Collaboration), JHEP **11**, 183 (2013)
[36] L. V. Bravina *et al.*, Eur. Phys. J. C **75**, 588 (2015)